crystals

MDPI

Article

Implications of Metamaterial on Ultra-Wide Band Microstrip Antenna Performance

Elham A. Serria and Mousa I. Hussein *

Department of Electrical Engineering, UAE University, Al Ain P.O. Box 15551, Abu Dhabi, UAE; 201470203@uaeu.ac.ae

* Correspondence: mihussein@uaeu.ac.ae

Received: 30 June 2020; Accepted: 1 August 2020; Published: 6 August 2020



Abstract: This study is addressing the slotted ring resonator effect on the performance of the ultra-wide band (UWB) microstrip antenna. Two types of metamaterial with double slotted ring resonators (SRR), circular (C-SRR) and square (S-SRR), are studied and implemented on back of the antenna. The design examines the effect of the number of the SRR and its position with respect to the antenna's ground plane and the rotation of the inner and outer C-SRR rings on different antenna characteristics. The dimensions of the antenna are 45 mm × 31 mm × 1.27 mm. The implementation of the SRR increased the antenna bandwidth to cover the range from 2.2 GHz to 9.8 GHz with rejected bands and frequencies. Antenna simulated characteristics like return loss, maximum gain and radiation pattern are obtained utilizing HFSS. The return loss measurement and the VSWR of the antenna with all SRR configuration studied are in good agreement with simulated results.

Keywords: microstrip antenna; metamaterial; SRR; circular SRR; square SRR; UWB

1. Introduction

Antennas are considered significant elements of any wireless communication system. An antenna is defined as a metallic structure used for transmitting and receiving signals or radio waves [1,2]. One of the most popular and utilized antenna types is the microstrip antenna that was first presented in 1950. The microstrip antenna is very prominent due to its small size, low price, simple structure, ease of fabrication and its capability to operate on multiple bands of frequencies; contrarily, it has some significant impediments such as very narrow frequency bandwidth, low efficiency, low power, false feed radiation and poor polarization purity [2,3].

With the high number of wireless devices in information epoch which depends on information transmission with higher data rate, provision security to consumers and business, increase the number of users, the importance of wideband wireless communication technology has increased rapidly [4,5]. UWB is defined as the technology of transmitting data over a broad bandwidth; with wireless transmission of −10 dB bandwidth is more than 25% of a center frequency or −10 dB bandwidth equal or larger than 1.5 GHz [6–8]. In 2002, the Federal Communication Commission (FCC) declared the authorization of using the unlicensed frequency band between 3.1 GHz to 10.6 GHz for commercial communication applications. FCC reserved bandwidth of 7.5 GHz for UWB due to its importance [8,9]. Due to the necessity of a low-cost solution for microwave communication systems and the growth in wireless applications, the idea of UWB microstrip antennas was getting noticed by researchers. Antenna researchers and designers have focused on variety of challenges in order to overcome the disadvantages of microstrip antennas. Farhood et al. [10] presented a hexagonal-shaped patch antenna of added two capacitive loaded line resonators (CLLRs) on the ground plane to achieve UWB bandwidth between 1.1 GHz to 10.69 GHz. Their antenna covers the UWB band from 3.1 GHz to 10.6 GHz and frequencies 2.4 GHz and 9.1 GHz for Bluetooth and radar applications. The designed antenna has

an omnidirectional radiation pattern. Kardile et al. [11] introduced a multiband circular microstrip antenna; their antenna consists of a circular patch and a microstrip feeding line with a notch that produces the multiple bands. A U-shaped slot was embedded onto the antenna patch to achieve band-stop filtering over the frequency range. The antenna has three bands from 1.5 GHz to 2.8 GHz, 3.3 GHz to 4.7 GHz and ultra-wideband characteristics from 6 GHz to 16.10 GHz. The antenna's maximum gain is 4.58 dB, and radiation efficiency is around 86.17%.

Furthermore, in [12], Sultan et al. introduced a double notched self-complementary UWB antenna. It consists of semi-ring with tapered section, T-shaped slot etched in the radiating patch and two C-shaped close to the microstrip feed line. Antenna's frequency bandwidth is between 2.2 GHz and 12 GHz, and the maximum gain is 3.5 dB; with radiation efficiency of 70%. New composite materials were introduced in the microwave and optics applications, known as a metamaterial, having unnatural properties [13]. Electromagnetic metamaterials are defined as efficient homogenous structures that have properties not found in nature [14]. In the late 60 s, V.G. Veselago proposed the idea of the metamaterial existence that had both negative electric permittivity ε and negative magnetic permeability μ simultaneously. In 1999, split-ring resonators (SRRs) were studied to provide negative magnetic permeability μ by Pendry [15]. SRR is defined as a sub-wavelength metamaterial structure that displays negative permeability μ over a narrow frequency band around its resonance frequency [16]. A double-ring SRR is another form of SRR, it is made of two concentric rings separated by a gap with splits at opposite sides; in this case, a resonant structure can be obtained [17]. Etching SRR on the ground plane of a microstrip antenna is used to modify antenna's performance. An SRR has been used extensively by many studies in the fields of antenna and microwave devices design. In many applications SRR has been introduced to enhance the performance of the device or suppress the device functionality at specific frequencies. In [18], Mahmud et al. introduced a microstrip antenna with a modified triangular patch, and two arrays of 2 × 4 square SRRs were placed on the radiating patch and ground plane. Their proposed antenna has a bandwidth from 3.1 GHz to 9 GHz, and gain increased more than 3 dBi. Research by Hamad et al. studied the UWB microstrip patch antenna with metamaterials of X-shaped slots on the radiating patch and ground plane, their design enhanced antenna's bandwidth to cover the range 3.2 GHz to 23.9 GHz, with a peak gain of 6.2 dB [19]. Islam et al. [20] designed the UWB antenna with a hexagonal split-ring resonator (HSRR) for sensing the PH factor in sensor application. The designed antenna covers the bandwidth between 3 GHz to 20 GHz and total antenna efficiency of 70% with a gain of 3.88 dB. Ebadzadeh et al. [21] proposed a UWB monopole antenna covering a frequency band from 3.1 GHz to 10.6 GHz with a notched band that occurs around 5 GHz to 6 GHz. This antenna operates for wireless local area networks (WLAN) due to SRR on the ground plane. In [22], UWB circular monopole antenna was studied, the antenna covers the entire UWB bandwidth 3.1 GHz to 10.6 GHz. Two rectangular shaped SRR were implemented to create a notched band between 6.41 GHz to 8.26 GHz for X-band satellite communication application. Li et al. [23], have used an array of a complimentary double-ring SRR on the conducting backplane of a square patch antenna with a single resonance frequency at 3.5 GHz. Their proposed design has resulted in a 22% size reduction, where as other antenna parameters, such as directivity and maximum gain were not affected by the introduction of the SRR. In another application Sharma and Sumeet [24] designed a fidget spinner-shaped antenna with four operating bands. Then the authors introduced a double circular SRR on the antenna side. The authors concluded that the introduction of the SRR helped to improve the impedance matching of antenna, which resulted in an improved reflection loss at the original operating band without the SRR. Abdelkebir et al. [25] implemented an artificial magnetic conductor surface with meander monopole antenna to improve antenna's electromagnetic performances.

This study investigates how different shapes and configurations of an SRR, mainly circular SRR (C-SRR) and square SRR (S-SRR) will alter the performance of an UWB circular microstrip antenna. The circular microstrip patch antenna and SRRS arrangements are simulated and assessed by ANSOFT's high-frequency structure simulator (HFSS V18). Measurements of selected designs that are fabricated

in UAEU labs will be discussed. It is expected that SRR will increase antenna's bandwidth and provides the possibility to transmit or reject specific frequencies bands based on SRR design parameters.

2. Antenna Design

A UWB microstrip antenna of circular patch with elliptical slot rings was designed. This antenna consists of a printed circular patch modified with elliptical slot rings excited by a rectangular edge-fed microstrip line. The circular patch design is selected for outer dimensions of antenna design due to its excellent radiation efficiencies, impedance bandwidth and omni-directional far-field beam pattern [26]. In this antenna, Rogers 5880-LZ substrate of a length 45 mm and a width of 31 mm is used with a dielectric constant of ε_r = 1.96, substrate thickness h = 1.27 mm and a loss tangent of 0.0009. Moreover, a partial conducting ground plane with a length of 11 mm and a width of 31 mm is implemented; the ground plane length of 11 mm was selected after performing several parametric simulations to produce the best wideband results. Fundamentally, three lunar slots are employed on the patch's circular shape to reduce the antenna reflection loss (S_{11}) and enhance the VSWR. Antenna's detailed geometry is demonstrated in Figure 1, Tables 1 and 2.

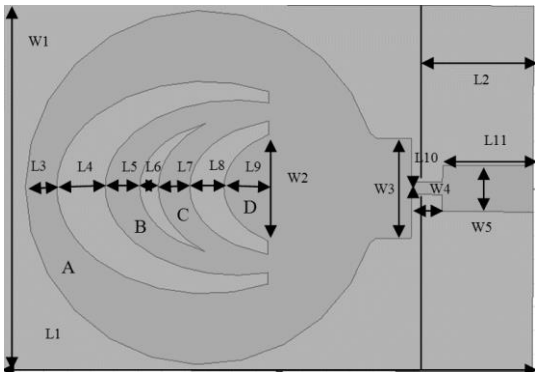


Figure 1. Circular antenna structure.

Table 1. Antenna dimensions.

Part	Length (mm)	Part	Length (mm)
L1	45.00	L9	4.900
L2	11.00	L10	2.650
L3	2.651	L11	7.680
L4	4.130	W1	31.00
L5	2.900	W2	9.000
L6	2.000	W3	8.480
L7	2.650	W4	1.030
L8	2.900	W5	3.920

Table 2. Ring specifications.

Ellipse	Major Radius (mm)	Ration
A	15.0	1
B	7.42	1.5
C	6.89	1.5
D	5.30	1.5

The parametric simulation was conducted on a ground length ranges between 8 mm–13 mm to achieve optimal design performance. Figure 2 shows the return loss with the ground plane variations, which in return affects the resonant frequency. As a consequence of the return loss value and UWB requirements, 11-mm length of the ground plane is noticeable to be the most appropriate value with

a frequency range between 3.5 GHz and 9 GHz; the best return loss obtained is −40 dB at 4.6 GHz, as illustrated in Figure 3. The VSWR of this design is less than two for the impedance bandwidth between 3.5 GHz and 9 GHz. The maximum gain obtained is almost 5 dB in the UWB band, as shown in Figure 4.

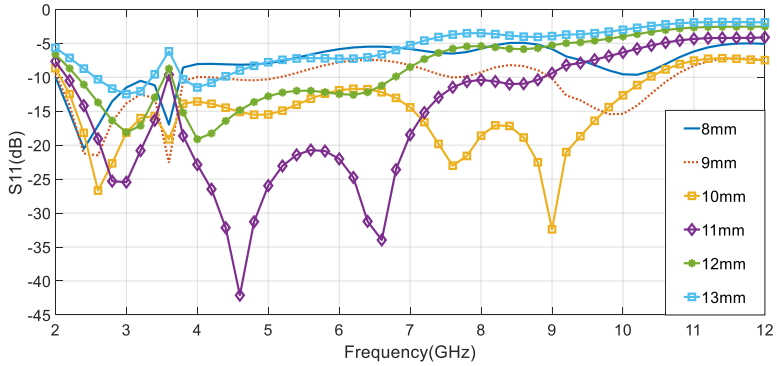


Figure 2. Simulated S_{11} for ground length 8–13 mm.

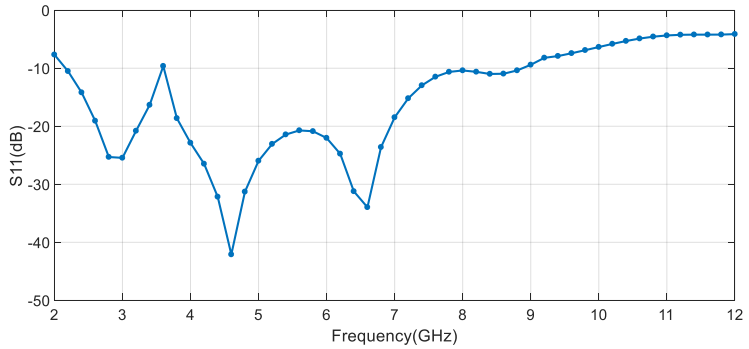


Figure 3. Simulated S_{11} for the optimal value of ground length 11 mm.

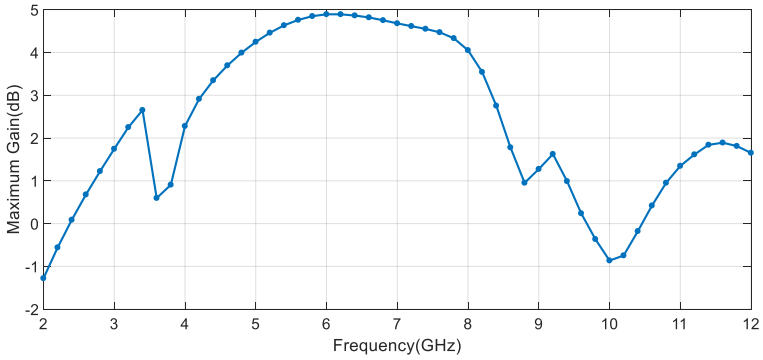
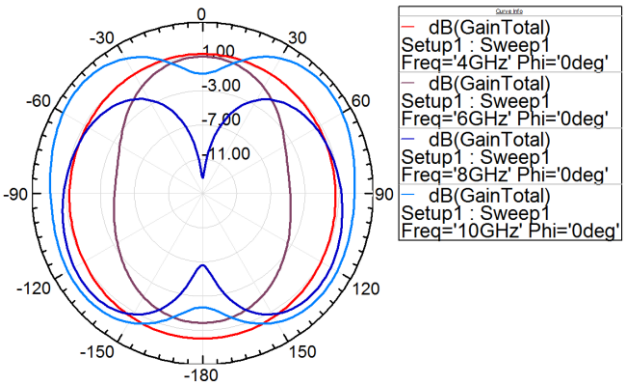
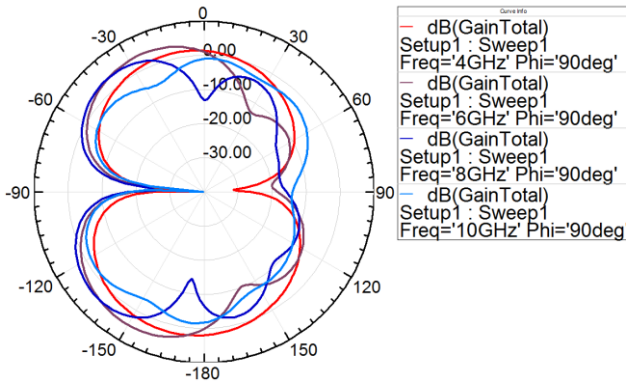


Figure 4. Simulated maximum gain.

Moreover, the radiation pattern is another essential antenna parameter; The proposed antenna's radiation pattern at different frequencies of 4 GHz, 6 GHz, 8 GHz and 10 GHz in both E- and H-planes are presented in Figure 5 at Phi = 0° and Phi = 90°. Obviously, the radiation pattern is almost omni-directional at Phi = 0° plane. The proposed antenna with 11 mm partial ground was fabricated and displayed in Figure 6. The return loss measurement shows that the antenna has a frequency bandwidth between 3.5 GHz and 8.4 GHz and a return loss up to −38 dB at 4.2 GHz, Figure 7. The simulated and measured results are in good agreement with a compression in the measured results between 5 GHz to 6 GHz. The small variation between the measured and simulated results can be attributed to the use of SMA-N adapter during the VNA calibration process. Overall, both results have acceptable performance over the design range.



(**a**) Phi = 0°



(**b**) Phi = 90°

Figure 5. Radiation pattern at Phi = 0° & 90°.



Figure 6. Fabricated circular microstrip antenna with elliptical rings.

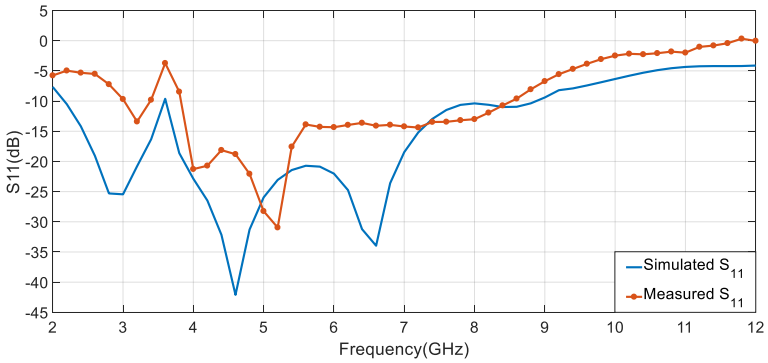


Figure 7. S_{11} for the fabricated microstrip antenna.

3. Metamaterials Design

The new idea of structured materials known as metamaterials was studied to benefit from its functionality and behavior. This material can produce new types of materials with negative electric permittivity, negative magnetic permeability and a negative refractive index [27]. Metamaterials are classified according to the properties of electric permittivity ε and magnetic permeability μ into four groups [28]: (1) double-positive (DPS) materials are materials with positive permittivity $\varepsilon > 0$ and positive permeability $\mu > 0$. Most of the materials in nature such as dielectrics belong to DPS; (2) epsilon negative (ENG) materials are materials that have negative permittivity $\varepsilon < 0$ and positive permeability $\mu > 0$ like plasmas. For microwave applications, thin metal wires are used to produce ENG material; (3) Mu-negative (MNG) materials are materials with positive permittivity $\varepsilon > 0$ and negative permeability $\mu < 0$. Gyrotropic material is an example of a material that has negative permeability, in addition, split-ring resonator (SRR) is the most widely used MNG material; (4) double negative (DNG) materials are materials that are not available in nature so it should be produced artificially. In this class both permittivity and permeability are negative $\varepsilon < 0$ and $\mu < 0$. SRR material with MNG properties was used extensively in antenna and microwave applications. In 1999, John Pendry proposed the double slotted ring resonator structure, where both rings are split [29]. SRRs have many geometric shapes, but in this study, the analysis will be concentrated on circular and square SRR.

A unit cell of double SRR structure consists of two concentric metallic rings with slots (gaps) at opposite sides; the two rings have a small separation between them and are made of nonmagnetic metal such as copper [30,31]. Exciting the SRR by a time-varying electromagnetic wave, with a magnetic field (H-field) is perpendicular to the plane of the SRR, this induces a current in the two rings. The two gaps on the opposite side prevent current flow around the rings but allow an induced current to flow on the ring surface and pass from one ring to the other as a displacement current through the capacitive split between the two rings. The high value of distributed capacitance on the gap between the two rings, which store the same amount of charges, but an opposite sign at both sides of the gap, prompts strong coupling between the two rings and lower the resonant frequency. The total capacitance of an SRR structure is the series distributed capacitance on the two rings and the two gaps capacitance [31–36]. Moreover, SRR inductance is specified according to the length of the rings and it is becoming larger when ring length increased; due to SRR capacitance and inductance, it behaves as a resonant LC circuit [34,35,37]. Figure 8 shows how the current flow on circular and square SRR.

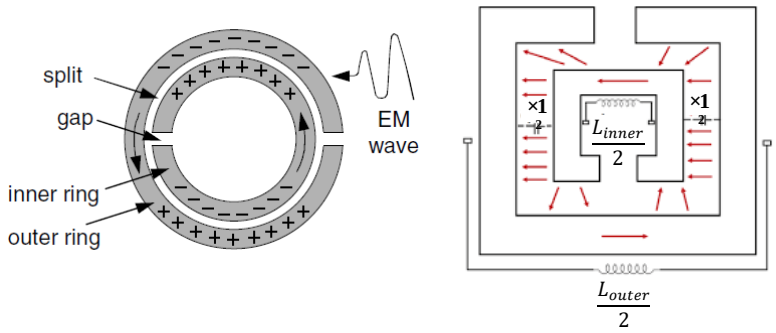


Figure 8. Electric current flow on split-ring resonators (SRRs).

SRR, circular and square, behaves as an LC resonator that can be excited by an electromagnetic field [38]; the equivalent LC circuit model is displayed in Figure 9; L_s is the resonator self-inductance and the two SRR rings have the capacitance in halves, $C_0/2$ [39]. SRR structure's total capacitance is the series capacitance of its two rings [35].

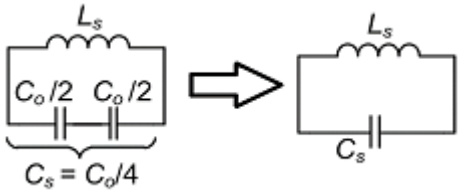


Figure 9. SRR equivalent circuit model.

From the equivalent circuit of the SRR, it can be noticed that the structure acts as an LC circuit with the resonant frequency specified by the total inductance and capacitance of the SRR structure [40]. In the next analysis, the designing equations and HFSS analysis for circular and square SRR are presented.

3.1. Circular SRR (C-SRR) and Square SRR (S-SRR) Design

Figure 10 shows the schematic view of circular SRR and its resonance frequency is expressed as:

$$\omega_0 = \sqrt{\frac{2}{(C_0 + C_g)L}} \tag{1}$$

where C_0 is the distributed capacitance, C_g is the gap capacitance and L is the self-inductance of the rings.

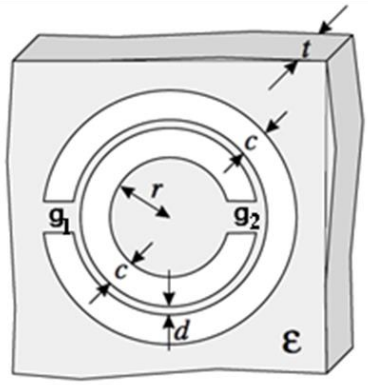


Figure 10. Schematic view of a circular split-ring resonator.

The resonant frequency of square SRR, demonstrated in Figure 11, is given by [41,42]:

$$f_0 = \frac{1}{2\pi}\sqrt{\frac{1}{L_T C_{eq}}} \tag{2}$$

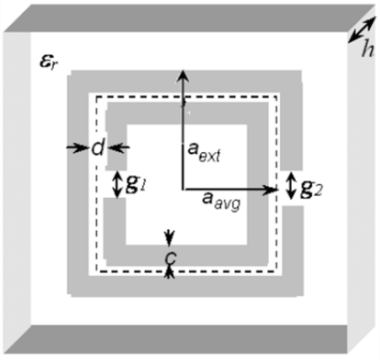


Figure 11. Schematic view of a square split-ring resonator.

L_T is the total inductance and C_{eq} is the total equivalent capacitance. For detailed C-SRR and S-SRR design equations, refer to references [29,34,35].

3.2. Circular and Square SRR Design Analysis

In order to analyze the behavior of SRR unit cell, all structures are designed using the same geometry in [36,41] and printed on Rogers 5880-LZ substrate with a dielectric constant of $\varepsilon_r = 1.96$, with dielectric loss tangent of $\tan\delta = 0.0009$ and substrate thickness of 1.27 mm. Parameters values of circular and square SRRs are shown in Table 3.

Table 3. Circular and square SRR unit cell parameters.

Circular SRR		**Square SRR**	
The Unit Cell Parameters	**Value (mm)**	**The Unit Cell Parameters**	**Value (mm)**
Ring width (c)	0.7	Ring width (c)	0.5
Ring thickness (h)	37 µm	Ring thickness (t)	35 µm
Inter – ring spacing (d)	0.2	Inter – ring spacing (d)	0.2
Split gap (g)	0.2	Split gap (g)	0.8
Substrate thickness (t)	1.27	Substrate thickness (h)	1.27
Inner ring radius (r)	2.2	Square half side (a_{ext})	2.6

The resonance behavior of the circular SRR, in Figure 12, has resonant frequencies at 3.6246 GHz, 13.5906 GHz and 19.7908 GHz, as displayed in Figure 13. It is noticeable that SRR has a resonance at different frequencies where it has a good transmission. A jumping phenomenon occurs at the resonant frequency where there is a phase change in (S_{11}), which confirms some material characteristics such as negative permeability. Figure 14 shows the behavior of the magnetic permeability of the proposed circular SRR. It is clearly shown that the permeability takes negative values at the transmission parameter (S_{21}). The surface current density for the circular SRR at the first resonant frequency 3.6246 GHz is shown in Figure 15; it is observed that most the current is concentrated at the inner side of each ring opposite to its gap and the same figure displays the direction of the surface current that flows in the same direction, clockwise, for the two rings.

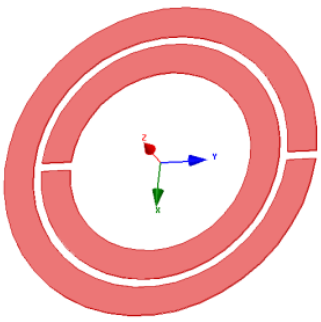


Figure 12. Circular SRR designed in HFSS.

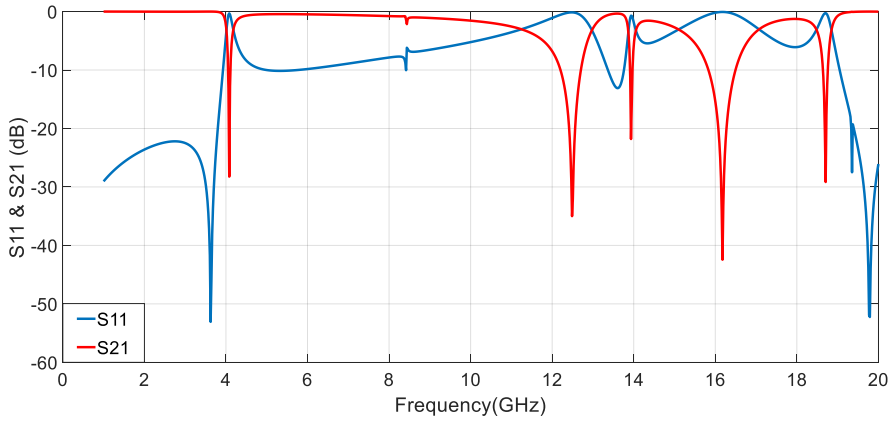


Figure 13. S_{11} and S_{21} for circular SRR.

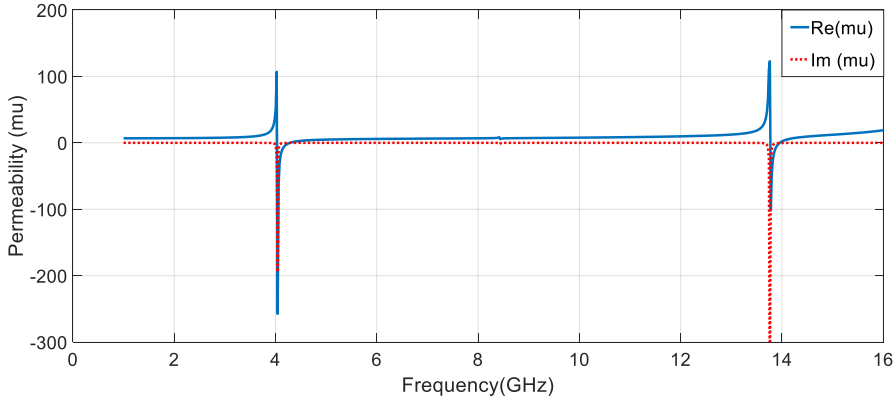


Figure 14. Real and imaginary effective permeability μ.

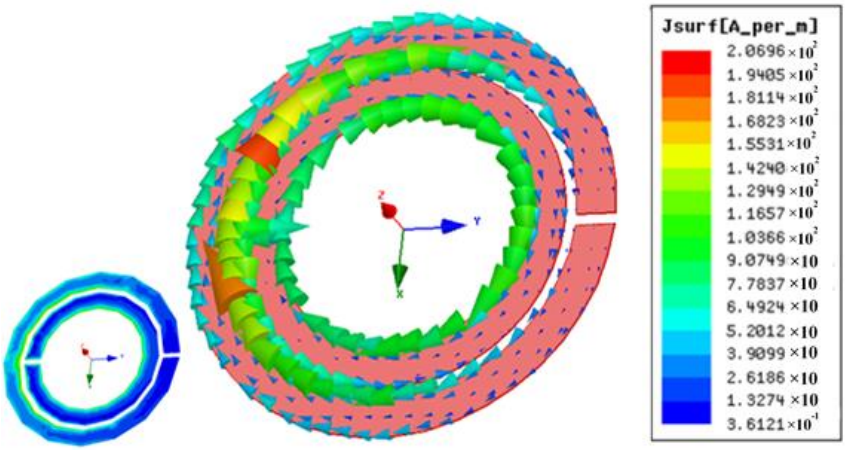


Figure 15. Surface current density and its vectors for circular SRR.

The next unit cell to be analyzed is the S-SRR, Figure 16, which has two resonant frequencies at 4.975 GHz and 17.6226 GHz, as displayed in Figure 17. At the transmission parameter S_{21}, the permeability of the square SRR is having a negative value, Figure 18. Metamaterial characteristic is shown clearly in the permeability behavior of changing from positive to negative values at specific frequency. The current concentration is at the inner side of each ring opposite to the gaps at resonant frequency 4.975 GHz, and the flow of the current for the two rings is in the same direction counter-clockwise, Figure 19.

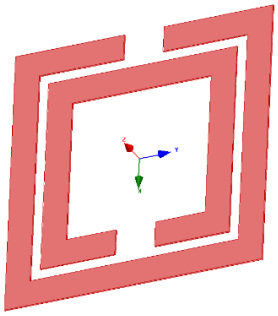


Figure 16. Square SRR designed in HFSS.

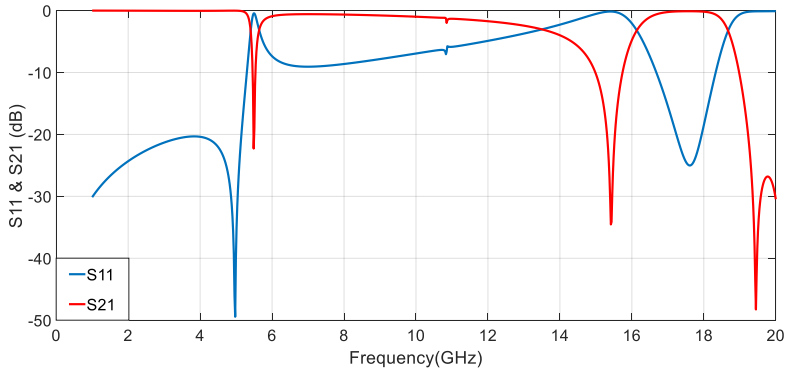


Figure 17. S_{11} and S_{21} for square SRR.

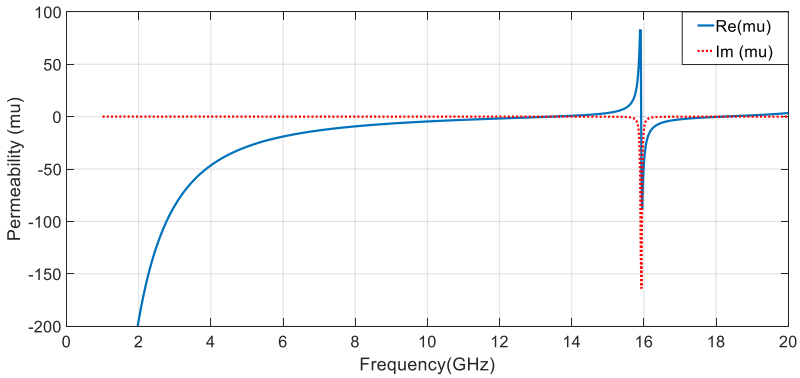


Figure 18. Real and imaginary effective permeability μ.

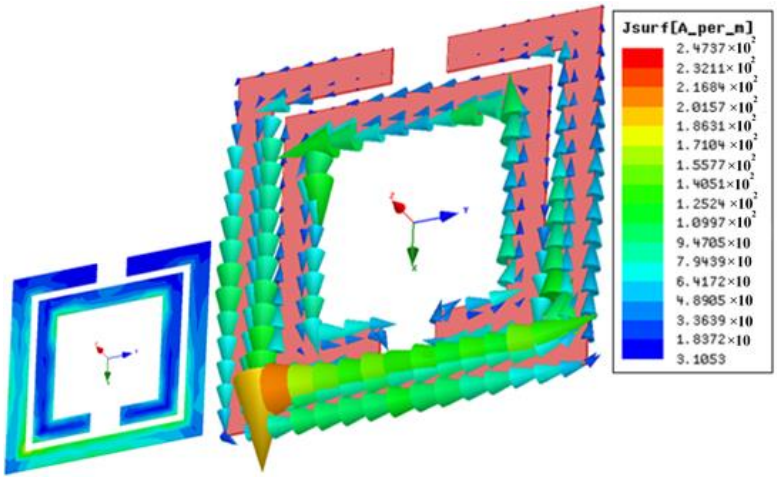


Figure 19. Surface current density and its vectors for square SRR.

4. Antennas Implemented with Metamaterials

4.1. Implementation of Circular-SRR

The UWB circular microstrip antenna with elliptical rings was combined with C-SRR to improve the antenna return loss and increase the bandwidth. The experiment started with implementing the same C-SRR with dimensions detailed in Table 3, on the back of the antenna (ground side of the substrate). Beginning with one C-SRR at the center (origin (0, 0)), then the number of C-SRRs are increased gradually; by this addition of C-SRRs, arrays of 3 × 2 and 3 × 3 are created. Figure 20 shows the implementations of different numbers of C-SRR, and the results are presented in Table 4 and Figure 21.

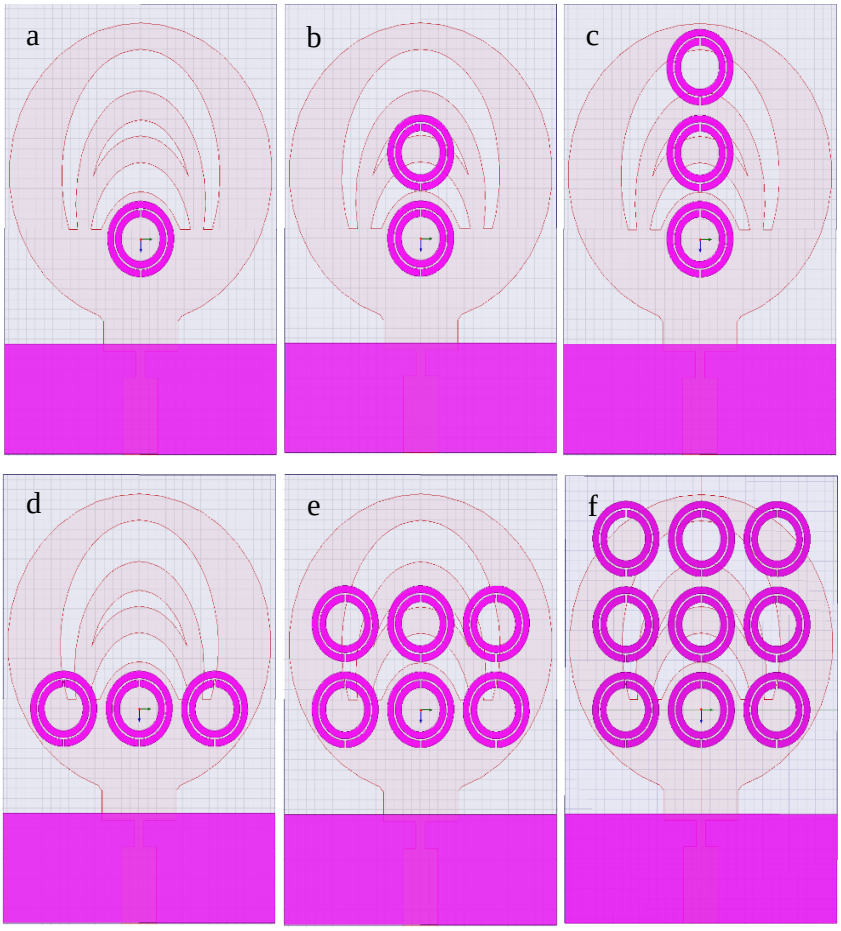


Figure 20. Different number of C-SRR on the back of the antenna. Arrays of (**a**) 1 × 1 (**b**) 1 × 2 (**c**) 1 × 3 (**d**) 3 × 1 (**e**) 3 × 2 (**f**) 3 × 3.

Table 4. Results of C-SRR implementations with the antenna.

Case	C-SRR No.	Frequency Bandwidth (GHz)	Return Loss (dB)
a	1	3.5–9	−42
b	2 on y-axis	3.5–8	−49.65
c	3 on y-axis	3.2–8.2	−40
d	3 on x-axis	2.2–8	−34.8
e	3 × 2	2.2–8	−33.74
f	3 × 3	2.8–8	−45.7

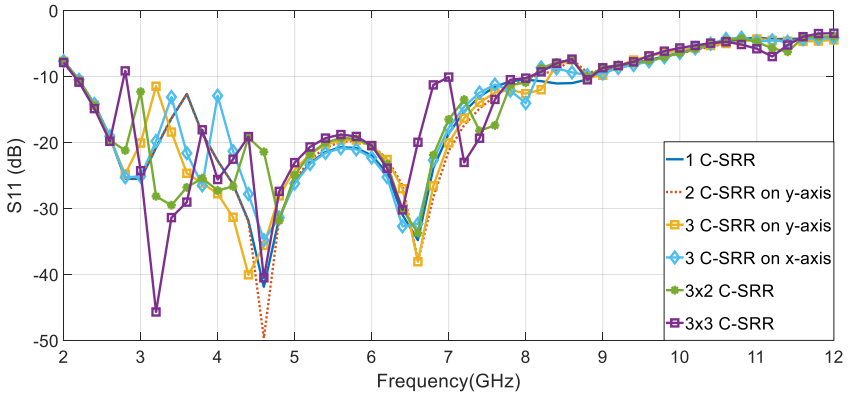


Figure 21. S_{11} for antenna with different number of C-SRR.

The return loss (S_{11}) of the circular antenna affected by increasing C-SRRs number was noticeable for 3 × 3 array while the lower numbers of C-SRRs have the no effect or small change enhancement occurs by implementing 3 × 3 C-SRR on the back of the antenna with a one-millimeter separation between each SRR unit, Figure 22. The effect of C-SRR on antennas return loss is shown in Figure 23. The introduction of the SRR resulted in a shift of the UWB start at 2.8 GHz and improved return loss over the entire band. The antenna's maximum gain is presented in Figure 24; it is almost 5 dB. The antenna's radiation pattern with implemented C-SRR is examined for different frequencies of 4, 6, 8 and 10 GHz with φ = 0° and 90°; it is noticeable that its radiation pattern has maintained omnidirectional behavior, Figure 25.

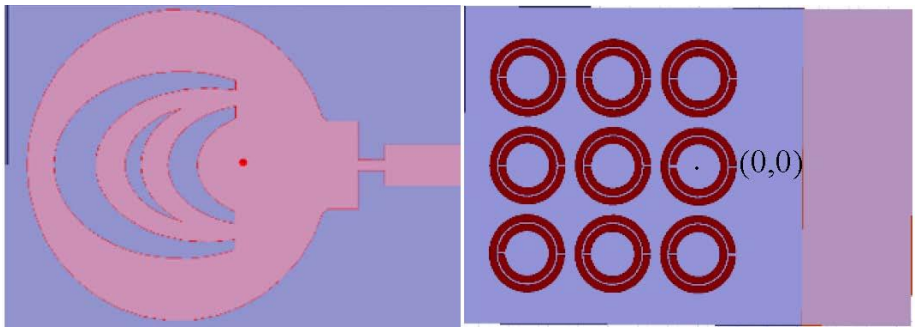


Figure 22. (**a**) Antenna front side (**b**) antenna back.

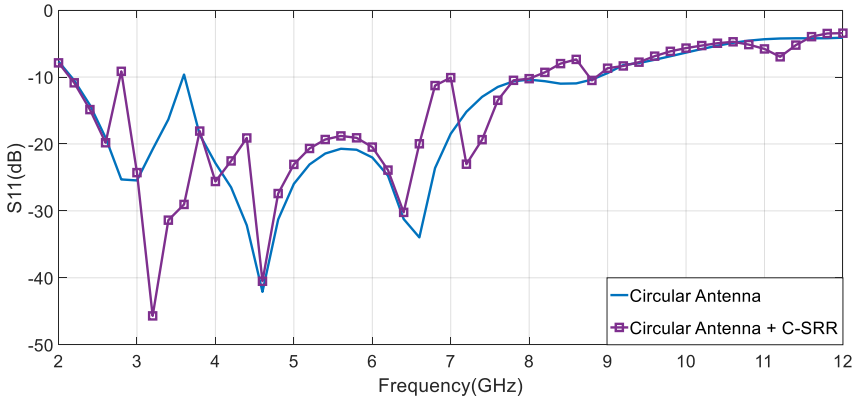


Figure 23. Simulated S_{11} for circular antenna and the antenna with 3 × 3 C-SRR.

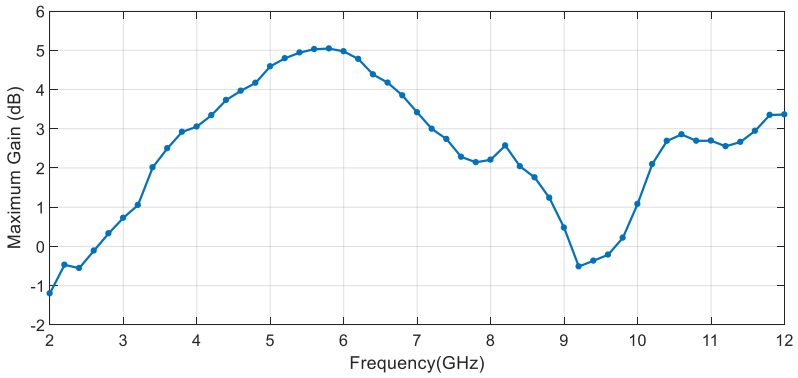
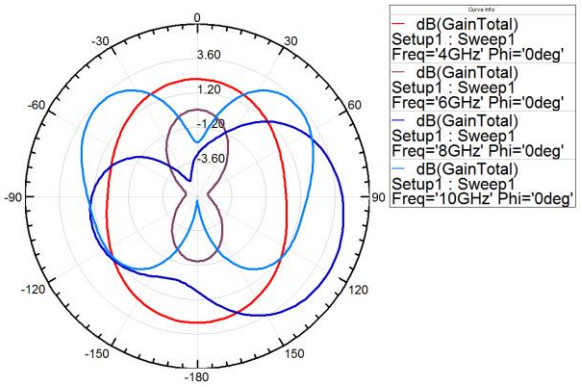
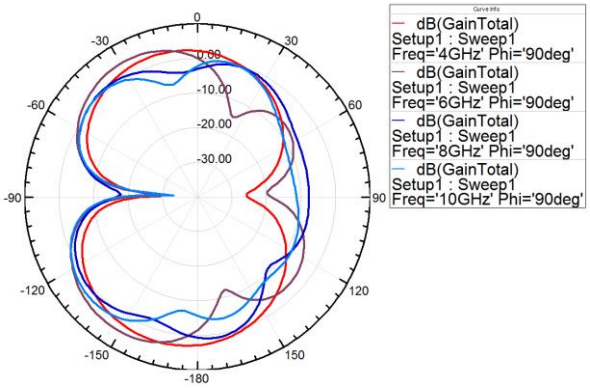


Figure 24. Simulated maximum gain for circular antenna with 3 × 3 C-SRR.



(**a**) Phi = 0°



(**b**) Phi = 90°

Figure 25. (**a**) Radiation pattern at Phi = 0° (**b**) radiation pattern at Phi = 90°.

The proposed circular microstrip antenna with an array of 3 × 3 C-SRR is fabricated in the lab and presented in Figure 26. The frequency bandwidth of the antenna is between 2.9 GHz to 8.8 GHz, Figure 27, with VSWR less than 2 for antenna's impedance bandwidth. The simulated and measured results are in good agreement.

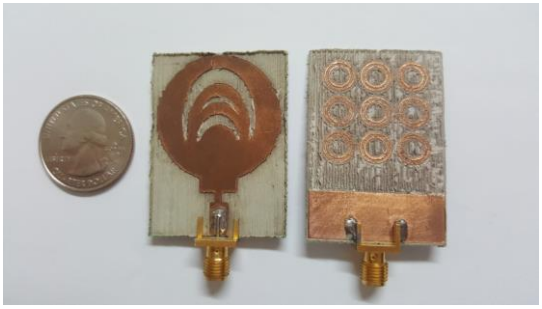


Figure 26. Circular microstrip antenna with C-SRR on the back.

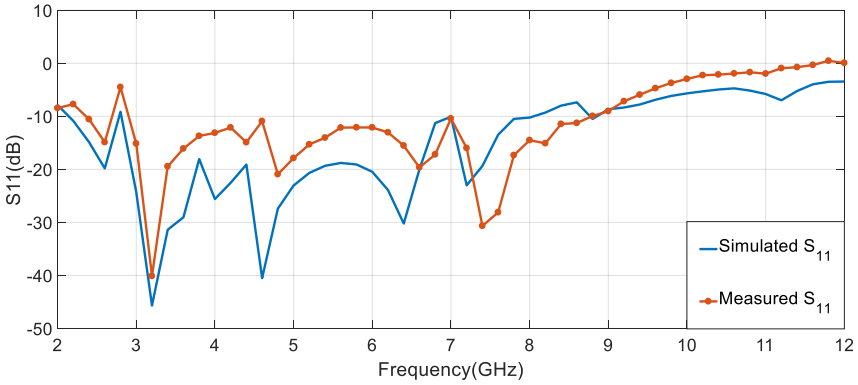


Figure 27. S_{11} for the fabricated antenna with C-SRR.

4.2. C-SRR and Ring Rotation

Studying the arrangements of the SRR double-ring orientation with respect to each other will provide an insight on the effect of the ring orientation on antenna's performance. Thus, Inner ring rotation of the SRR effect is investigated. Inner ring rotation of 10°, 3° and 17° is applied along either the row or the column configuration of the array. Figure 28 presents the antenna with SRR in case 1, where the rotation angles applied to the rows of the array. Case 2 displays the SRR arrangement along the column of the array. Figure 28 shows the return loss results with inner ring rotation, which results in a rejection or notched band from 3.91 GHz to 4.25 GHz for rotation along the row. On the other hand. Implementing ring rotation along the column resulted in a rejection bandwidth from 4.82 GHz to 5.6 GHz, as shown in Figure 29. Antenna's gain in case 1, case 2, is around 5 dB as displayed in Figure 30.

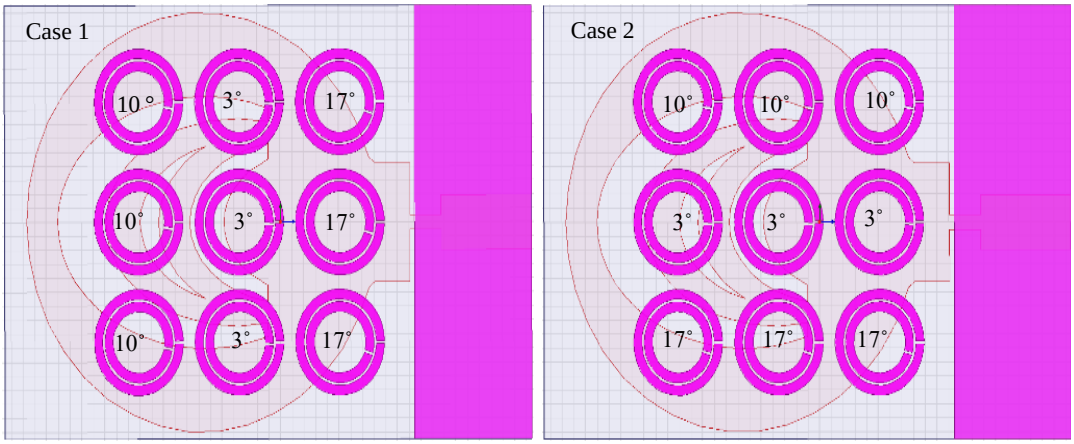


Figure 28. Inner ring rotation for C-SRRs.

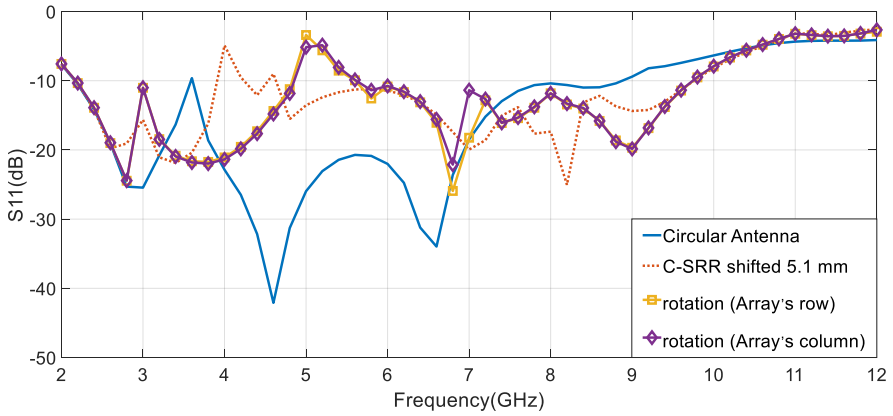


Figure 29. S_{11} for the antenna of shifted C-SRR and inner ring rotation horizontally and vertically.

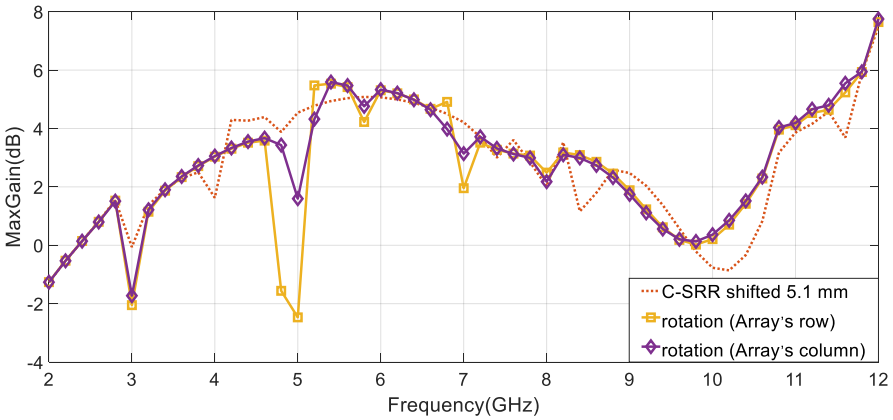


Figure 30. Maximum gain of the three antennas.

The next step for applying rotated inner rings will utilize positive (clockwise) and negative (anti-clockwise) angles rotation as displayed in Figure 31. Three cases are studied: Case 1: inner ring rotations for 47°, 33° and 10° are applied to the array's column on the back of the antenna. Such arrangement resulted in a rejection at three frequencies 4.8 GHz, 5.4 GHz and 7 GHz, Figure 32. In Case 2 negative angle rotation of −47° is implemented on the upper row, and the other two rows have positive angle rotation of 33° and 10°, respectively. This design has no rejection frequencies in its bandwidth, Figure 32. In Case 3 all SRRs are implemented with negative angles rotation of −47°, −33° and −10°. Figure 32 shows two rejection frequencies at 4.8 GHz and 7.2 GHz. The three designs have an improved frequency bandwidth between 2.2 GHz to 9.8 GHz and a maximum gain around 5.3 dB, Figure 33.

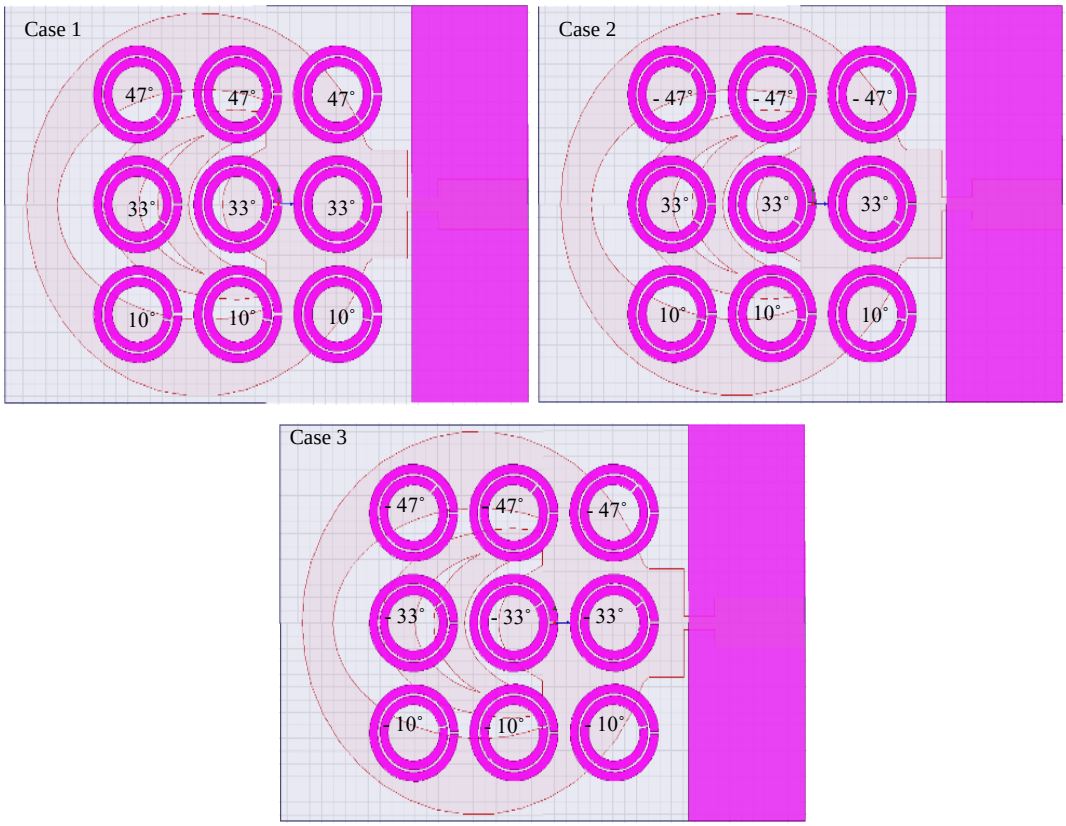


Figure 31. C–SRRs inner ring rotation for positive and negative angle.

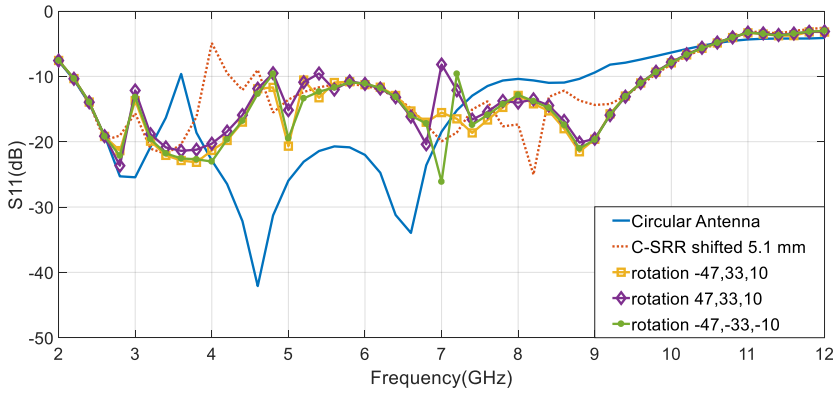


Figure 32. S_{11} of C-SRRs inner ring rotation for positive and negative angles.

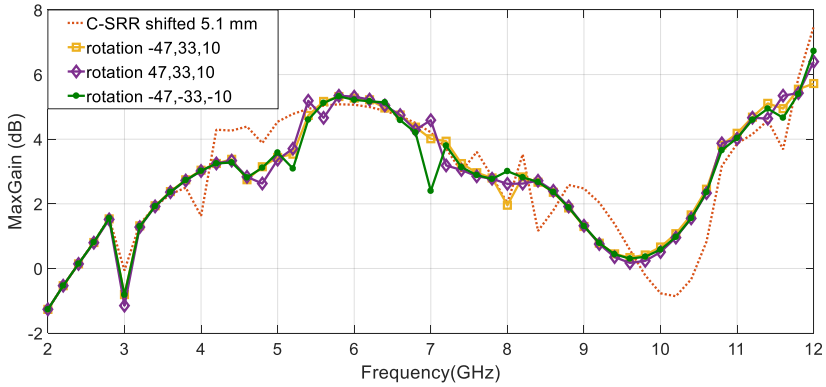


Figure 33. Maximum gain of the antennas.

The final C-SRR implementation is to study inner and outer ring rotation with positive/negative angles. Three cases are investigated with angle rotation of 7°, 13° and 30° as illustrated in Figure 34. The three studied cases are as follows: Case 1: angles 7°, 13° and 30° are applied the inner rings. In the scenario the antenna has two rejection frequencies at 4.8 GHz and 5.4 GHz, Figure 35. In Case 2 the same rotation angles 7°, 13° and 30° are used for outer ring. In this case the antenna did not exhibit any rejection bands, Figure 35. For Case 3: negative angles −7°, −13° and −30° are implemented on the outer rings, this implementation resulted in rejection bandwidth between 4.69 GHz to 5.44 GHz and a second rejection frequency at 7 GHz as depicted in Figure 35. The three design cases have an improved bandwidth from 2.2 GHz to 9.8 GHz. The antenna gain for the 3 cases is between 5.4 dB and 5.55 dB, as shown in Figure 36.

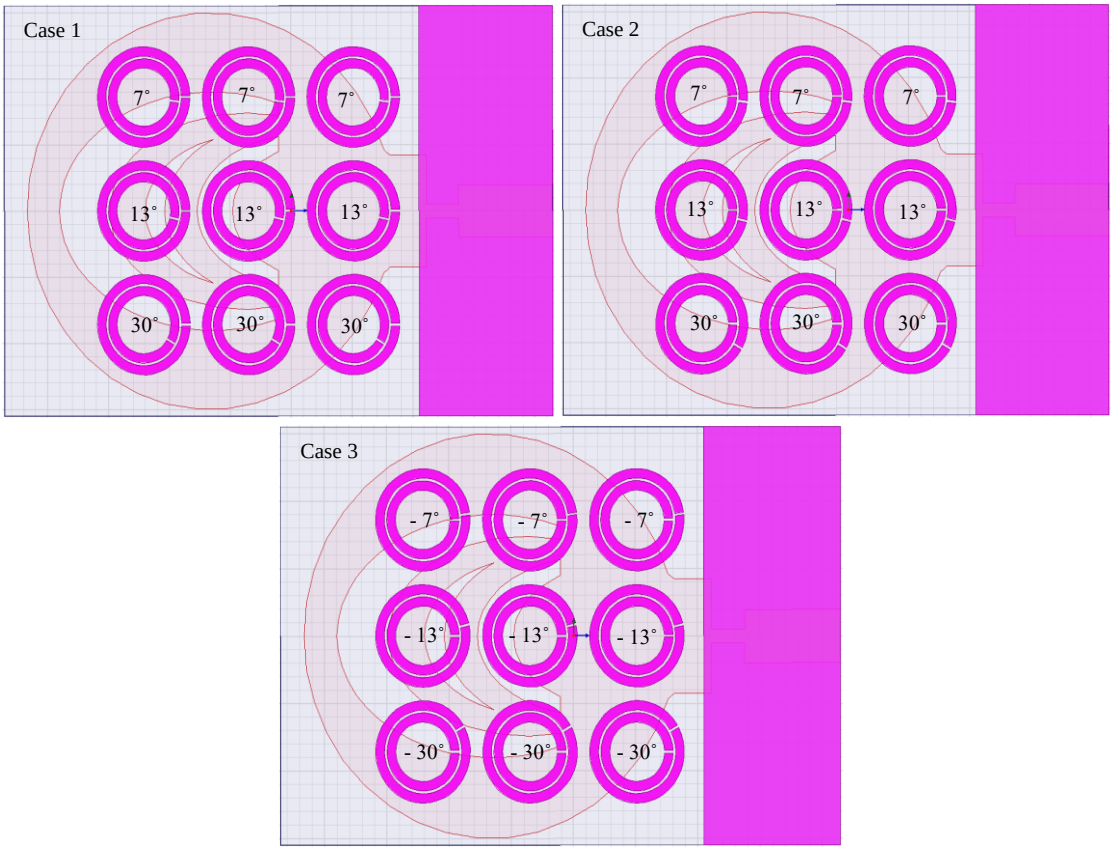


Figure 34. Inner and outer ring rotation for positive and negative angles.

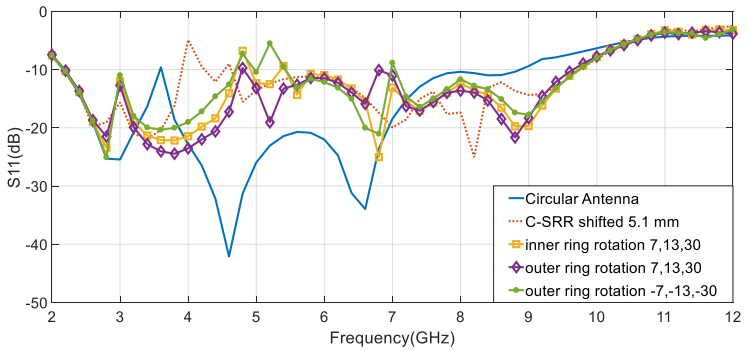


Figure 35. S_{11} for multiple C-SRR variations.

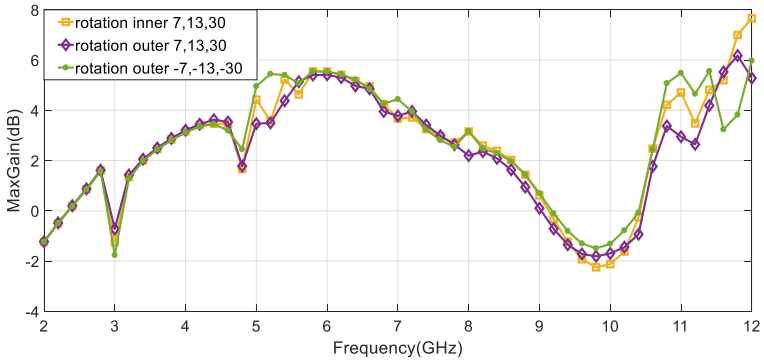


Figure 36. Antennas maximum gain.

The circular antenna, with rotated inner ring angles of 47°, 33° and 10° is fabricated in the lab and displayed in Figure 37. The measurement shows that the antenna has frequency bandwidth between 3.4 GHz and 9.4 GHz as shown in Figure 38; with VSWR is less than 2 in its bandwidth range. The simulated bandwidth is wider than the measured one, but both results are in good agreement.



Figure 37. Inner ring rotation.

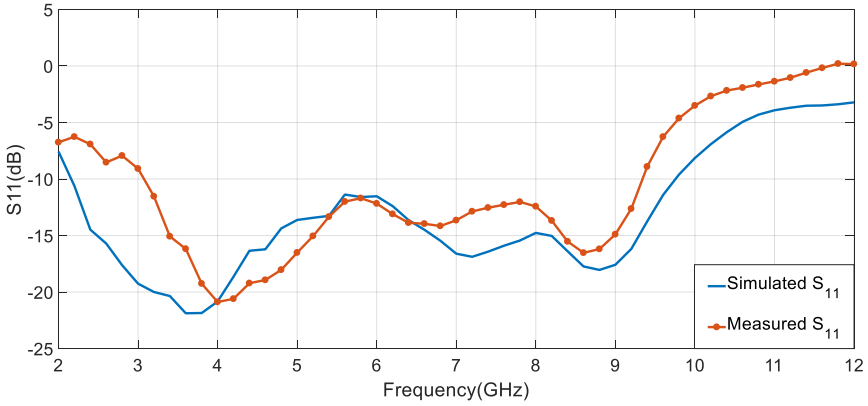


Figure 38. Simulated and measured S_{11}.

4.3. Implementation of Square-SRR

The S-SRR has been utilized in many antenna and microwave applications; such that, to design multi-band and single frequency notch filters and reduce the UWB antenna interference [41]. In this section, we study the effect of the array size on the antenna performance. The analysis starts with 2×1 array and increases up to 2×5 array size as shown in Figure 39a–e. The return loss results and

geometric configuration for all arrays 2 × 1–2 × 5 are presented in Figure 40 and Table 5. Maximum gain for the circular antenna with the S-SRR implementation of the studied arrays is around 5 dB; the gain is 4.897 dB for 2 × 1 and increased up to 5.053 dB for 2 × 5, Figure 41. The simulated radiation pattern of the antenna with the 2 × 4 array of the double S-SRR, Figure 42, shows that the antenna exhibits an omnidirectional radiation pattern and low gain at the rejection frequency 5.6 GHz.

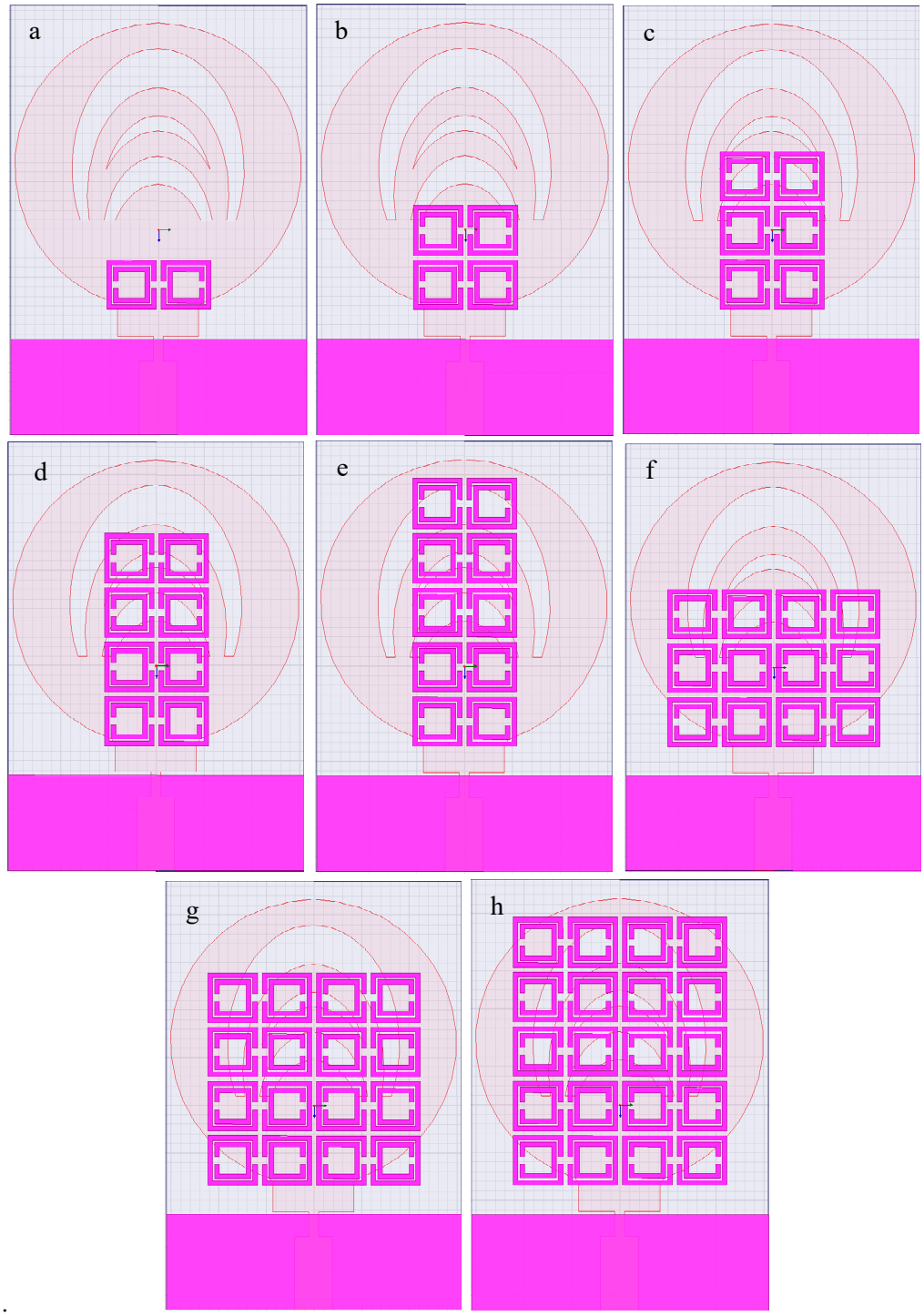


Figure 39. Implementation of S-CRR arrays. (**a**) 2 × 1 (**b**) 2 × 2 (**c**) 2 × 3 (**d**) 2 × 4 (**e**) 2 × 5 (**f**) 3 × 4 (**g**) 4 × 4 (**h**) 4 × 5.

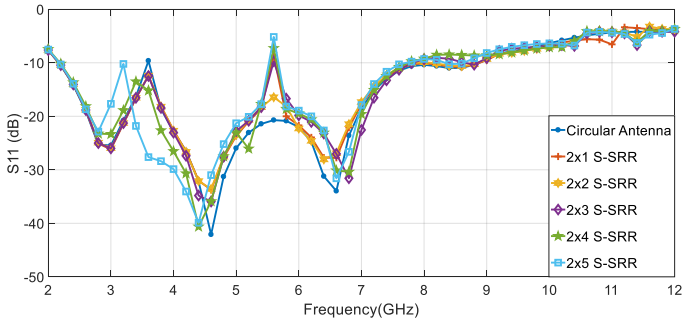


Figure 40. S_{11} for different S-SRR arrays.

Table 5. Results of S-SRR arrays implementations with the antenna.

Case	Array	Bandwidth (GHz)	Rejected Bands/Freq. (GHz)
a	2×1	2.2–9	5.6
b	2×2	2.2–9	-
c	2×3	2.2–8	5.6
d	2×4	2.2–8	5.6
e	2×5	2.2–8	5.6
f	3×4	2.2–10	4.85–5.8
g	4×4	2.2–10	4.85–5.8
h	4×5	2.2–10	4.85–5.8

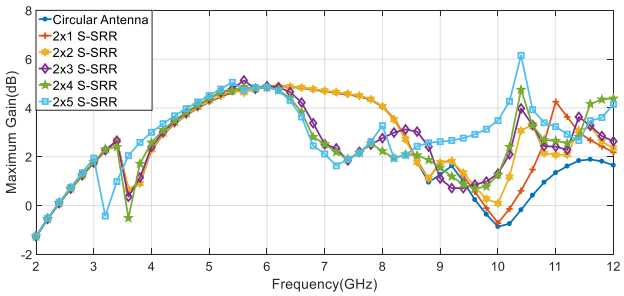
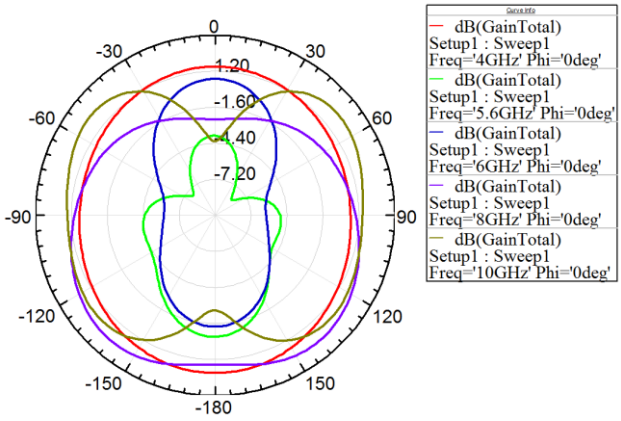
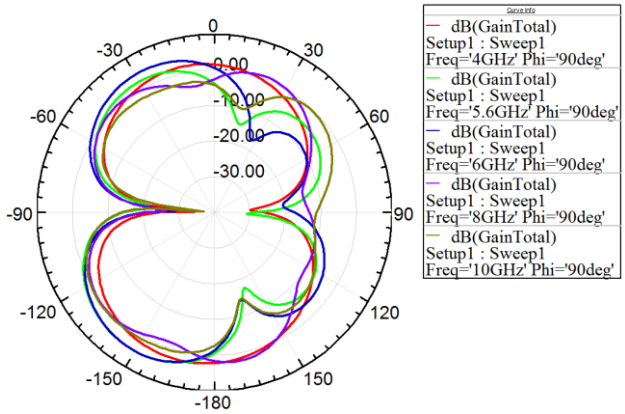


Figure 41. Antennas maximum gain with different S-SRR arrays.

The previous array size increased to 3×4, 4×4 and 4×5 as illustrated in Figure 39f–h. The three arrays have an improved frequency bandwidth from 2.2 GHz to 10 GHz with a notched band from 4.85 GHz to 5.8 GHz; with almost 1 GHz rejection band, Figure 43. The antenna maximum gain for all 3 arrays is around 5.2 dB as shown in Figure 44. The proposed antenna of 3×4 array has an omnidirectional radiation pattern at 4, 5, 5.2, 6, 8 and 10 GHz except for 5.6 GHz as this frequency located in the rejection band.



(**a**) **Phi = 0°**



(**b**) **Phi = 90°**

Figure 42. Radiation pattern for 2 × 4 array, (**a**) Phi = 0° (**b**) Phi = 90°.

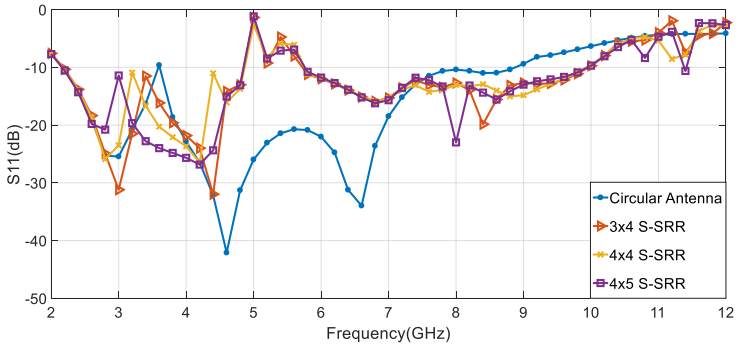


Figure 43. S_{11} for 3 × 4, 4 × 4 and 4 × 5 S-SRR.

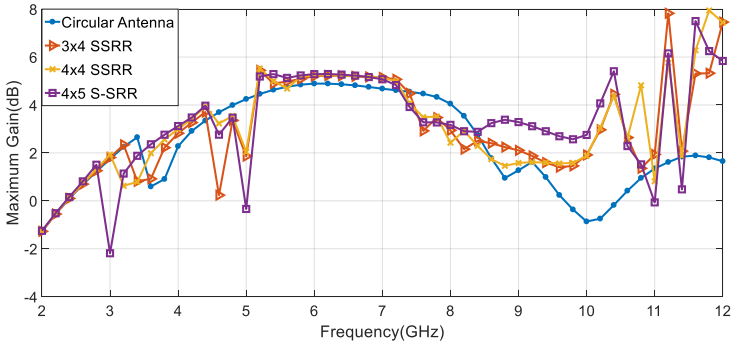


Figure 44. Antenna maximum gain with 3 × 4, 4 × 4 and 4 × 5 S-SRR.

5. Conclusions

UWB circular microstrip antenna with elliptical rings was designed covering bandwidth between 3.5 GHz to 9 GHz. In order to enhance the antenna performance, multiple techniques used based on implementing metamaterials SRR. Arrays with different structure and position with respect to the UWB antenna were investigated. The study covered two types of double-ring SRR, these are C-SRR and S-SRR. The C-SRR array effect is noticed on antenna's behavior, such as increasing the frequency bandwidth to be 2.2 GHz to 9.8 GHz with rejection bands and frequencies. Additionally, C-SRR ring rotation was investigated; rotation resulted in a larger bandwidth, exhibited frequency band rejection, increased antenna gain and could obtain multiple rejection frequencies. A similar performance was observed with the implementation of the S-SRR array structure. Other designs of SRR can be analyzed and implemented; different designs have different resonant frequencies, which will affect the antenna's performance. This study will open the door for future investigation of tunable array configuration to suite desired metamaterial applications. Furthermore, antenna's width and length, patch shape, the radius of a circular patch, patch slots and ground size are parameters that affect the whole performance of the antenna. In this case, the antenna can be selective and operates at other frequency bands rather than UWB.

Author Contributions: Conceptualization, M.I.H. and E.A.S.; methodology, M.I.H. and E.A.S.; software, E.A.S.; validation, M.I.H. and E.A.S.; formal analysis, E.A.S.; investigation, E.A.S.; resources, M.I.H.; data curation, E.A.S.; writing—original draft preparation, E.A.S.; writing—review and editing, M.I.H.; visualization, E.A.S.; supervision, M.I.H.; project administration, M.I.H.; funding acquisition, M.I.H. All authors have read and agreed to the published version of the manuscript.

Funding: This research received no external funding.

Conflicts of Interest: The authors declare no conflicts of interest.

References

1. Stutzman, W.L.; Thiele, G.A. *Antenna Theory and Design*; John Wiley and Sons: Hoboken, NJ, USA, 1981.
2. Balanis, C.A. *Antenna Theory Analysis and Design*, 3rd ed.; John Wiley and Sons: Hoboken, NJ, USA, 2005.
3. Misra, G.; Agarwal, A.; Agarwal, K. Design and Performance Evaluation of Microstrip Antenna for Ultra-Wideband Applications Using Microstrip Feed. *Am. J. Electr. Electron. Eng.* **2015**, *3*, 93–99.
4. Azim, R.; Islam, M.T. Printed Wide Slot Ultra-Wideband Antenna. In *Advancement in Microstrip Antennas with Recent Applications*; IntechOpen: London, UK, 2013; pp. 153–171.
5. Islam, M.T.; Azim, R. Recent Trends in Printed Ultra-Wideband (UWB) Antennas. In *Advancement in Microstrip Antennas with Recent Applications*; IntechOpen: London, UK, 2013; pp. 173–201.
6. Commission, F.C. *Revision of Part 15 of the Commission's Rules Regarding Ultra-Wideband Transmission Systems-First Report and Order*; Federal Communications Commission: Washington, DC, USA, 2002.
7. Foerster, J.; Green, E.; Somayazulu, S.; Leeper, D. Ultra-Wideband Technology for Short- or Medium-Range Wireless Communications. *Intel Technol. J. Q2* **2001**, *5*, 1–11.

8. Chandrana, A.A.; Thankachanb, S. Triple Frequency Notch in UWB Antenna with Single Ring SRR loading. In Proceedings of the 6th International Conference on Advances in Computing & Communications, ICACC, Kochi, India, 6–8 September 2016.
9. Haraz, O.; Sebak, A.R. UWB Antennas for Wireless Applications. In *Advancement in Microstrip Antennas with Recent Applications*; IntechOpen: London, UK, 2013; pp. 125–152.
10. Farhood, A.D.; Naji, M.K.; Rhaif, S.H.; Ali, A.H. Design and analysis of dual band integrated hexagonal shaped microstrip UWB antenna. *Indones. J. Electr. Eng. Comput. Sci.* **2019**, *15*, 294–299. [CrossRef]
11. Kardile, V.; Yadav, P.; Mishra, A. Design of Multiband Circular Microstrip Patch Antenna. *Int. Res. J. Eng. Technol. (IRJET)* **2016**, *3*, 1961–1963.
12. Sultan, K.S.; Dardeer, O.M.A.; Mohamed, H.A. Design of Compact Dual Notched Self-Complementary UWB Antenna. *Open J. Antennas Propag.* **2017**, *5*, 99–109. [CrossRef]
13. Xiong, H.; Hong, J.-S.; Tan, M.-T.; Li, B. Compact Microstrip Antenna with Metamaterial for Wideband Applications. *Turk. J. Electr. Eng. Comput. Sci.* **2013**, *21*, 2233–2238. [CrossRef]
14. Chandrasekaran, K.T.; Karim, M.F.; Alphones, A. Composite Right/Left-handed Structure based High Impedance Surface for Performance Enhancement of Planar Antennas. *IET Microw. Antennas Propag.* **2017**, *11*, 818–826. [CrossRef]
15. Bautista, F.H.; Vargas, C.A.; Arcos, J.M.V. Negative Refractive Index in Split Ring Resonators. *Materials* **2013**, *59*, 141–146.
16. Orten, P.Y.; Ekmekci, E.; Sayan, G.T. Equivalent Circuit Models for Split-ring Resonator Arrays. In Proceedings of the Progress in Electromagnetics Research Symposium, Cambridge, MA, USA, 5–8 July 2010; pp. 534–537.
17. Balmaz, P.G.; Martina, O.J.F. Electromagnetic Resonances in Individual and Coupled Split-Ring Resonators. *J. Appl. Phys.* **2002**, *92*, 2929–2936. [CrossRef]
18. Mahmud, M.Z.; Islam, M.T.; Misran, N.; Singh, M.J.; Mat, K. A Negative Index Metamaterial to Enhance the Performance of Miniaturized UWB Antenna for Microwave Imaging Applications. *Appl. Sci.* **2017**, *7*, 1149. [CrossRef]
19. Hamad, E.K.I.; Nady, G. Bandwidth Extension of Ultra-wideband Microstrip Antenna Using Metamaterial Double-side Planar Periodic Geometry. *Electromagn. Radio Eng.* **2019**, *28*, 25–32. [CrossRef]
20. Islam, M.T.; Ashraf, F.B.; Alam, T.; Misran, N.; Mat, K.B. A Compact Ultrawideband Antenna Based on Hexagonal Split-Ring Resonator for pH Sensor Application. *Sensors* **2018**, *18*, 2959. [CrossRef] [PubMed]
21. Ebadzadeh, S.R.; Zehforoosh, Y. A Compact UWB Monopole Antenna with Rejected WLAN Band using Split-Ring Resonator and Assessed by Analytic Hierarchy Process Method. *J. Microw.* **2017**, *16*, 592–601. [CrossRef]
22. Apoorva. Designing of Circular Monopole Patch Antenna Loaded with Split Ring Resonator. *Int. J. Adv. Res. Electr. Electron. Instrum. Eng.* **2017**, *6*, 1–10.
23. Li, R.; Zhang, Q.; Kuang, Y.; Chen, X.; Xiao, Z.; Zhang, J. Design of a Miniaturized Antenna Based on Split Ring Resonators for 5G Wireless Communications. In Proceedings of the Cross Strait Quad-Regional Radio Science and Wireless Technology Conference (CSQRWC), Taiyuan, China, 18–21 July 2019.
24. Sharma, N.; Bhatia, S.S. Metamaterial Inspired Fidget Spinner-Shaped Antenna Based on Parasitic Split Ring Resonator for Multi-Standard Wireless Applications. *J. Electromagn. Waves Appl.* **2020**, *34*, 1471–1490. [CrossRef]
25. Abdelkebir, S.; Mayouf, A.; Mayouf, F.; Zoubiri, B.; Devers, T. Study of Metamaterial Surface Wave Antenna Based on Split Ring Resonator. *Microsyst. Technol.* **2019**, *25*, 797–810. [CrossRef]
26. Srifi, M.N.; Podilchak, S.K.; Essaaidi, M.; Antar, Y.M.M. Compact Disc Monopole Antennas for Current and Future Ultrawideband (UWB) Applications. *IEEE Trans. Antennas Propag.* **2011**, *59*, 4470–4480. [CrossRef]
27. Ramakrishna, S.A. Physics of Negative Refractive Index Materials. *Rep. Prog. Phys.* **2005**, *68*, 449–521. [CrossRef]
28. Singh, G.; Ni, R.; Marwaha, A. A Review of Metamaterials and its Applications. *Int. J. Eng. Trends Technol. (IJETT)* **2015**, *19*, 305–310. [CrossRef]
29. Solymar, L.; Shamonina, E. *Waves in Metamaterials*; Oxford University Press: New York, NY, USA, 2009.
30. Castro, P.J.; Barroso, J.J.; Neto, J.P.L. Experimental Study on Split-Ring Resonators with Different Slit Widths. *J. Electromagn. Anal. Appl. (JEMAA)* **2013**, *5*, 366–370. [CrossRef]

31. Al Nuaimi, M.K.T.; Whittow, W.G. Compact Microstrip Band Stop Filter Using SRR and CSSR: Design, Simulation and Results. In Proceedings of the European Conference on Antennas and Propagation (EuCAP 2010), Barcelona, Spain, 12–16 April 2010.
32. Bulu, I.; Caglayan, H.; Aydin, K.; Ozbay, E. Compact Size Highly Directive Antennas Based on the SRR Metamaterial Medium. *New J. Phys.* **2005**, *7*, 1–10. [CrossRef]
33. Patel, S.K.; Kosta, Y. Triband Microstrip-Based Radiating Structure Design Using Split Ring Resonator and Complementary Split Ring Resonator. *Microw. Opt. Technol. Lett.* **2013**, *55*, 2219–2222. [CrossRef]
34. Aripin, Z.; Najmurrokhman, K.A.; Munir, A. Compact SRR-based Microstrip BPF for Wireless Communication. In Proceedings of the 2nd International Conference on Information Technology, Computer and Electrical Engineering (ICITACEE), Semarang, Indonesia, 16–18 October 2015.
35. Marqués, R.; Mesa, F.; Martel, J.; Medina, F. Comparative Analysis of Edge- and Broadside-Coupled Split Ring Resonators for Metamaterial Design—Theory and Experiments. *IEEE Trans. Antennas Propag.* **2003**, *51*, 2572–2581. [CrossRef]
36. Barroso, J.J.; Castro, P.J.; Neto, J.P.L. Experiments on Wave Propagation at 6.0 GHz in a Left-Handed Waveguide. *Microw. Opt. Technol. Lett.* **2010**, *52*, 2175–2178. [CrossRef]
37. Kar, S.; Ghosh, M.; Kumar, A.; Majumder, A. Complementary Split Ring Resonator-Loaded Microstrip patch Antenna Useful for Microwave Communication. *Int. J. Electron. Commun. Eng.* **2016**, *10*, 1321–1325.
38. Baena, J.D.; Bonache, J.; Martín, F.; Sillero, R.M.; Falcone, F.; Lopetegi, T.; Laso, M.A.G.; García, J.G.; Gil, I.; Portillo, M.F.; et al. Equivalent-Circuit Models for Split-Ring Resonators and Complementary Split-Ring Resonators Coupled to Planar Transmission Lines. *IEEE Trans. Microw. Theory Tech.* **2005**, *53*, 1451–1461. [CrossRef]
39. Ballesta, F.A.; Gil, M.; Sindreu, M.D.; Bonache, J.; Martin, F. Characterization of Metamaterial Transmission Lines with Coupled Resonators through Parameter Extraction. In *Metamaterial*; Jiang, X.Y., Ed.; InTech Open Science|Open Minds: London, UK, 2012; pp. 303–320.
40. Saha, C.; Siddiqui, J.Y. Theoretical Model for Estimation of Resonance Frequency of Rotational Circular Split-Ring Resonators. *Electromagnetics* **2012**, *32*, 345–355. [CrossRef]
41. Saha, C.; Siddiqui, J.Y.; Antar, Y.M.M. Square Split Ring Resonator Backed Coplanar Waveguide for Filter Applications. In Proceedings of the URSI General Assembly and Scientific Symposium, Istanbul, Turky, 13–20 August 2011.
42. Bahl, I.; Bhartia, P. *Microwave Solid State Circuit Design*, 2nd ed.; John Wiley and Sons: Hoboken, NJ, USA, 2003.



© 2020 by the authors. Licensee MDPI, Basel, Switzerland. This article is an open access article distributed under the terms and conditions of the Creative Commons Attribution (CC BY) license (http://creativecommons.org/licenses/by/4.0/).